

Two-dimensional MoS₂ electromechanical actuators

Nguyen T. Hung¹, Ahmad R. T. Nugraha¹, Riichiro Saito¹

¹Department of Physics, Tohoku University, Sendai 980-8578, Japan

E-mail: nguyen@flex.phys.tohoku.ac.jp

February 2014

Abstract. We investigate electromechanical properties of two-dimensional MoS₂ monolayers in the 1H, 1T, and 1T' structures as a function of charge doping by using density functional theory. We find isotropic elastic moduli in the 1H and 1T structures, while the 1T' structure exhibits an anisotropic elastic modulus. Moreover, the 1T structure is shown to have a negative Poisson's ratio, while Poisson's ratios of the 1H and 1T' are positive. By charge doping, the monolayer MoS₂ shows a reversibly strain and work density per cycle ranging from -0.68% to 2.67% and from 4.4 to 36.9 MJ/m³, respectively, making them suitable for applications in electromechanical actuators. Stress generated is also examined in this work and we find that 1T and 1T' MoS₂ monolayers relatively have better performance than 1H MoS₂ monolayer. We argue that such excellent electromechanical performance originate from the electrical conductivity of the metallic 1T and semimetallic 1T' structures high Young's modulus of about $150 - 200$ GPa.

1. Introduction

Natural muscle is an example of good-performance actuator with work cycles involving contractions of more than 20%, although the stress generation ability of natural muscle is quite low (0.35 MPa) [1] compared with mechanical machine. Various actuation materials have been studied to replace natural muscle that can directly convert electrical energy into mechanical energy, with wide potential applications in soft robotics, adaptive wings for aircraft, and biometric machines [1]. Some well-known actuation materials, such as carbon nanotubes (CNTs) [2, 3] and graphene [4, 5], were shown to generate larger stress than natural muscle and also larger strain ($\sim 1\%$) than ferroelectric materials (0.1 – 0.2%) due to their high Young's moduli of about 1 TPa [6, 7]. Recently, Weissmuller et al. [8, 9] showed that Au-Pt alloys with a network of nanometer-sized pores are good candidates for the actuation materials because the linear strain reaches $\sim 1.3\%$ and work density per cycle is up to 6 MJ/m³, which is a performance indicator of the muscle. However, the use of CNTs, graphene, and Au-Pt nanoporous metal as the electromechanical actuator materials are still limited mainly because such actuator materials are expensive and there are difficulties in synthesis, which also make the development of artificial muscle quite stagnant.

Very recently, Acerce et al. [10] showed a significant performance on the electromechanical actuation of two-dimensional metallic molybdenum disulfide (MoS₂) nanosheet. The MoS₂ nanosheet is able to generate mechanical stresses of about 17 MPa and strains of about 0.8%, which leads to the work density for freely actuated MoS₂ films of about 81 kJ/m³. The MoS₂ nanosheet actuator is also able to lift more than 150 times its own weight at low voltages ± 0.3 V for hundreds of cycles. High actuation performance of the 1T MoS₂ nanosheet originates from the high electrical conductivity of the metallic 1T structure and their elastic modulus of 2.5 GPa. However, their study is limited to the 1T MoS₂ nanosheet (or the multilayer MoS₂) although it is known that MoS₂ could have at least three different stable forms that have been synthesized so far: 1H, 1T, and 1T' phases [11, 12]. Furthermore, the condition of charge doping that can possibly support for high actuation performance of the *monolayer* MoS₂ layers is still unclear in both experimental and theoretical investigations.

With the above backgrounds, it is highly desirable to explore the strain, stress, work density and electronic structure of two-dimensional MoS₂ under the charge doping to understand the best conditions or the best structures for electromechanical actuator, which can be evaluated by first-principles calculations. Theoretically, it is expected that *monolayer* MoS₂ has higher electrical conductivity and larger surface area than the MoS₂ nanosheet [13–15]. Therefore, in this work we will focus our attention on the electromechanical actuator performance of the 1H, 1T, and 1T' MoS₂ monolayers as a function of charge doping for both electron and hole doping. As the main highlight of this paper, our calculated results reveal that the 1T and 1T' MoS₂ monolayers relatively have better performance and better actuator response than 1H MoS₂ monolayer. In addition, depending on the structure, we can have either isotropic or anisotropic actuation

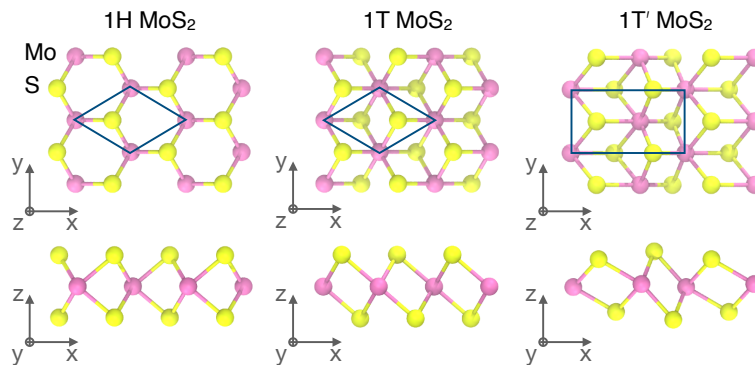


Figure 1. Top and side views of 1H, 1T, and 1T' structures of monolayer MoS₂. The 1H, 1T, and 1T' structures are composed of trigonal, octahedral and distorted octahedral lattices, respectively.

properties in the MoS₂ monolayers.

2. Method

2.1. Calculation details

In Fig. 1, we show the 1H, 1T, and 1T' structures of the monolayer MoS₂. The 1H MoS₂ structure is based on trigonal lattice, where the S atoms are located in a hexagonal close-packed structure while the Mo atoms are sandwiched between two atomic layers of S atoms in a trigonal prismatic geometry. In the cases of 1T MoS₂ and 1T' MoS₂, the Mo atoms are octahedrally ordered and disordered, respectively, surrounded by the S atoms. The primitive unit cells of the 1H and 1T MoS₂ are hexagonal with the optimized lattice parameters of 3.19 Å and 3.18 Å, respectively, while the unit cell of the 1T' MoS₂ is rectangular with the optimized lattice parameters of $a = 5.72$ Å and $b = 3.16$ Å as shown in Fig. 1. These lattice parameters are consistent with previous theoretical results [16,17]. Since periodic boundary condition is applied in all models, a vacuum space of 30 Å in the direction perpendicular to the monolayer (z direction) is used in order to avoid virtual interactions between layers.

We perform first-principles calculations to determine the total energy and the electronic structure of monolayer MoS₂ using the Quantum ESPRESSO package [18]. We use pseudopotentials from the Standard Solid-State Pseudopotentials library (accuracy version) [19]. The exchange-correlation energy is evaluated by the general-gradient approximation using the using the Perdew-Burke-Ernzerhof functional [20]. An energy cut-off of 60 Ry is chosen for the expansion of the plane waves, which is sufficient to obtain convergence of total energy. In our simulation, the \mathbf{k} -point grids in the Brillouin-zone are employed according to the Monkhorst-Pack scheme [21], where \mathbf{k} is the electron wave vector. We use $16 \times 16 \times 1$, $16 \times 16 \times 1$, and $8 \times 16 \times 1$ \mathbf{k} -points for the 1H, 1T and 1T' MoS₂, respectively. To obtain optimized atomic configurations of MoS₂ monolayers, the atomic positions and cell vectors are fully relaxed using the

Broyden-Fletcher-Goldfarb-Shanno minimization method [22–25] until all the Hellmann-Feynman forces and all components of the stress are less than 5×10^{-4} Ry/a.u. and 5×10^{-2} GPa, respectively.

To discuss the electromechanical actuation of the MoS₂ monolayers, the geometry optimization is then performed for each charge doping from -0.1 to $+0.1$ electron per atom (e/atom), in which the electron (hole) doping is simulated by adding (removing) electrons to the unit cell with the same amount of uniformly positive (negative) charge in the background so as to keep the charge neutrality.

2.2. In-plane mechanical moduli

In order to obtain mechanical moduli of MoS₂ monolayers, we firstly calculate elastic constants C_{ij} , which are derived from the finite difference approach by using the Thermo-pw code [26]. From the point of view of elasticity theory, it is known that the values of C_{ij} are related to the equivalent volume of the unit cell. Because a vacuum space is left along the z direction in the unit cell, the calculated C_{ij} must be rescaled by h/d_0 , where h is the length of the cell along z axis and d_0 is the effective layer thickness of the monolayer MoS₂. In the present study, we set $d_0 = 6.145 \text{ \AA}$ i.e., one half of the out-of-plane lattice constant of bulk MoS₂ [27]. The angular dependence of the in-plane (xy -plane) Young's modulus $Y(\theta)$ and Poisson's ratio $\nu(\theta)$ are then expressed as [28]

$$Y(\theta) = \frac{C_{11}C_{22} - C_{12}^2}{C_{11}\alpha^4 + C_{22}\beta^4 - \left(2C_{12} - \frac{C_{11}C_{22} - C_{12}^2}{C_{66}}\right)\alpha^2\beta^2}, \quad (1)$$

and

$$\nu(\theta) = \frac{C_{12}(\alpha^4 + \beta^4) - \left(C_{11} + C_{22} - \frac{C_{11}C_{22} - C_{12}^2}{C_{66}}\right)\alpha^2\beta^2}{C_{11}\alpha^4 + C_{22}\beta^4 - \left(2C_{12} - \frac{C_{11}C_{22} - C_{12}^2}{C_{66}}\right)\alpha^2\beta^2}, \quad (2)$$

where θ is the angle relative to the x direction, $\alpha = \sin(\theta)$, $\beta = \cos(\theta)$, and C_{ij} are the elastic constants obtained from the first-principles calculations. Since monolayer MoS₂ is a two-dimensional structure, there are four independent elastic constants C_{11} , C_{22} , C_{12} , and C_{66} .

2.3. Work-per-cycle analysis

As an important performance indicator for actuation, we adopt the work density per cycle W of an actuator for discussion of the monolayer MoS₂. We assume that the actuator is a linear elastic solid and the general condition to be considered is illustrated in Fig. 2. There are three states when the actuator is loaded by a constant tensile force: (1) the material is at zero charge doping $q = 0$ with an initial length L_0 , (2) applying a charge doping $q \neq 0$ produces a length change L_A due to the electromechanical actuation

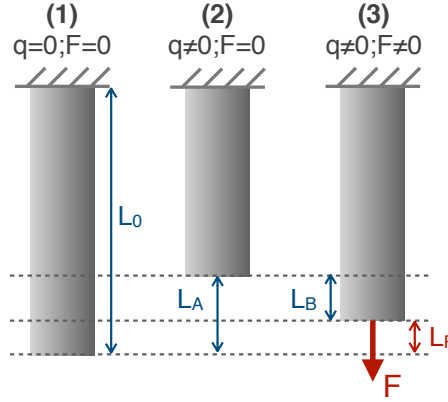


Figure 2. Length changes occurring during the loading and actuation processes.

process, and (3) applying a force $F \neq 0$ produces a deformation L_B . According to Hooke's law, which is generally true at small strains, L_A and L_B are given by

$$L_A = \epsilon L_0, \quad L_B = \frac{FL_0}{AY}, \quad (3)$$

where ϵ , Y , and A are, respectively, the strain, Young's modulus, and cross-sectional area of monolayer MoS₂ after the charge doping has been applied. The work density per cycle that includes steps (1)-(3) as shown in Fig. 2 is given by [29]

$$W = \frac{F(L_A - L_B)}{V}, \quad (4)$$

where $V = L_0 A$ is the volume. By substituting L_A and L_B in Eq.3 into Eq.4, W can be written as

$$W = \frac{F\epsilon}{A} - \frac{F^2}{A^2 Y}. \quad (5)$$

We can determine the maximum W from Eq.5 by solving $dW/dF = 0$. The formula for the maximum work density per cycle is given by

$$W_{\max} = \frac{1}{4} Y \epsilon^2, \quad (6)$$

when $F_{\max} = \frac{1}{2} Y \epsilon A$. However, in most of experiments, the work density is often expressed in terms of stored energy density W_s , which is calculated from the linear relation between σ and ϵ , giving the formula

$$W_s = \frac{1}{2} Y \epsilon^2 = 2W_{\max}. \quad (7)$$

Equation 7 will be used to compare our theoretical results with recent experimental data of MoS₂ electromechanical actuators [10].

3. Results

3.1. Mechanical properties

To discuss the actuator response of the monolayer MoS₂, we firstly check the mechanical moduli at the neutral condition and at the charge doping cases. In Fig. 3a, we show the

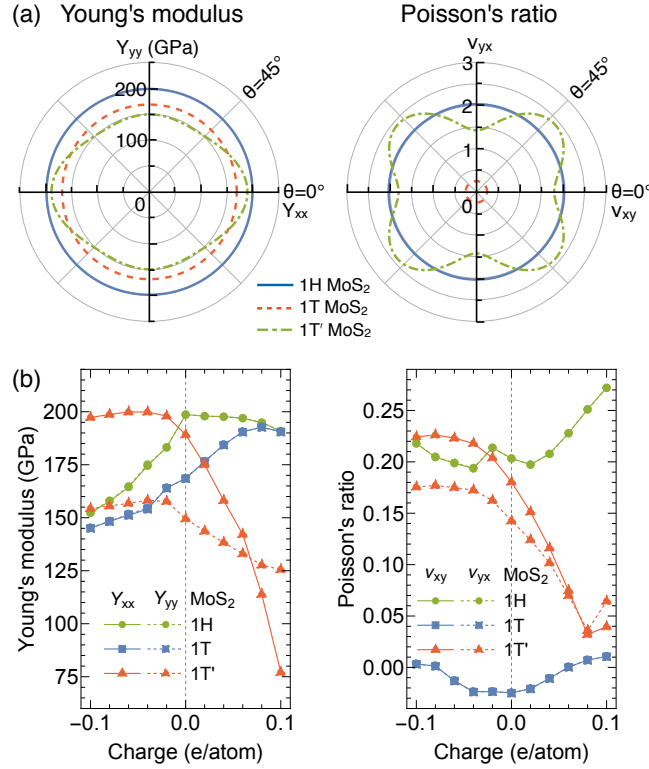


Figure 3. (a) Polar diagram for Young's modulus Y (left) and Poisson's ratio ν (right) of monolayer MoS₂ with 1H, 1T, and 1T' structures. The angle θ identifies the direction of applied force with respect to the x -axis. Isotropic (anisotropic) behaviour is associated with a circular (noncircular) shape of the polar plot. (b) Young's modulus and Poisson's ratio of monolayer MoS₂ plotted as function of charge doping per atom.

Table 1. Elastic constants C_{ij} (GPa), Young's modulus Y (GPa) and Poisson's ratio ν of the monolayer MoS₂ with 1H, 1T, and 1T' structures.

MoS ₂	C_{11}	C_{22}	C_{12}	C_{66}	Y_{xx}	Y_{yy}	ν_{xy}	ν_{yx}
1H	207	207	42	83	197	197	0.20	0.20
1T	169	169	-4	86	167	167	-0.02	-0.02
1T'	194	153	28	61	189	150	0.18	0.14

dependences of Y and ν on the direction of monolayer MoS₂ at the neutral condition, i.e. $q = 0$. The shape of Y and ν in the polar plot indicates not only the elastic isotropy in the 1H and 1T MoS₂ monolayers, but also the elastic anisotropy in the 1T' MoS₂ monolayer. The anisotropy of elastic moduli in the 1T' MoS₂ monolayer originates from the fact that the low-symmetry 1T' structure is a distorted one from the high-symmetry 1T structure. For comparison, the values of C_{ij} , Y , and ν of the 1H, 1T and 1T' MoS₂ structures are listed in Table 1. We can see that Y is found to be 199 GPa for the 1H MoS₂, which is in a good agreement with a previous theoretical result ($Y = 200$ GPa) [13]. Bertolazzi et al. [14] obtained an effective Y of 270 ± 100 GPa for the monolayer MoS₂, while Castellanos-Gomez et al. [15] obtained an average Y of $210 - 370$ GPa for multilayer MoS₂ consisting of 5 to 25 layers. Note that both experiments [14,15] using atomic force

microscope tip applied on the monolayer or multilayer MoS₂ suspended on the substrate containing an array of circular holes are under biaxial tensile stress. Therefore, the experimental results of biaxial elastic modulus are higher than the theoretical results of uniaxial elastic modulus in this present study. We obtained the Young modulus $Y = 167$ GPa for the 1T MoS₂, while $Y_{xx} = 189$ GPa and $Y_{yy} = 150$ GPa for the 1T' MoS₂.

The values of Poisson's ratio of the monolayer MoS₂ are unique because the 1T structure exhibits a negative Poisson's ratio of -0.02 , while Poisson's ratios of the 1H ($\nu = 0.20$) and 1T' MoS₂ ($\nu_{xy} = 0.18$ and $\nu_{yx} = 0.14$) are positive. When a compressive (tensile) strain is acted in one direction, materials tend to expand (contract) in the perpendicular direction, corresponding to positive Poisson's ratio for ordinary materials. The opposite is the situation for materials with negative Poisson's ratio. We note that beside our study, there have been reports that Poisson's ratio can be negative in other 2D materials such as in black phosphorus ($\nu = -0.5$) [30], single-layer graphene ribbons ($\nu = -1.51$) [31], and δ -phosphorene ($\nu = -0.267$) [32]. We expect that exploring 2D materials with negative Poisson's ratio could have useful applications, for example, as vanes for aircraft gas turbine engines, sponges, and fasteners [33].

In Fig. 3b, we show Y and ν of the monolayer MoS₂ as a function of charge doping, i.e. $q \neq 0$. For the electron doping ($q < 0$), Y of the 1H and 1T structures is decreased, while Y of the 1T' structure is increased. For the hole doping ($q > 0$ e/atom), Y of 1T' structure is increased, while Y of the 1H and 1T structures decreased. The maximum Y of monolayer MoS₂ of about 200 GPa is smaller than that of carbon-based structures (400 – 1000 GPa) [3, 34], but is comparable to that of stainless steel (192 GPa) [35]. The high Y values of monolayer MoS₂ are important for artificial muscle applications since it could generate large force per unit area. Moreover, a significant change of ν is found in the 1T' structure from 0.23 to 0.03, as shown in Fig. 3b. For the 1H and 1T structures, ν increases with increasing $|q|$ for both electron and hole doping. It should be noted that Poisson's ratio of the 1T structure becomes positive at $q = -0.08$ e/atom ($\nu = 0$) and at $q = 0.06$ e/atom ($\nu = 0$) for the electron and hole doping, respectively.

3.2. Actuator response

In order to study the variation of the structural deformation as a function of charge doping, we define the in-plane strain as

$$\epsilon_{xx} = \Delta a/a_0, \quad \epsilon_{yy} = \Delta b/b_0, \quad (8)$$

where a_0 and b_0 are, respectively, the length of the unit cell in x and y directions at geometry optimization for neutral case, and Δa and Δb are the increment (or decrement) of a_0 and b_0 , respectively, after the charge doping has been applied. In Fig. 4, we show the strain for each monolayer MoS₂ as a function of charge doping q ranging from -0.1 to 0.1 e/atom. This charge range is reasonable because a typically accessible charge in experiments is ranging from -0.3 to 0.1 e/atom [36]. In the neutral case, we obtain strains $\epsilon_{xx} = \epsilon_{yy} = 0$. For the electron doping, i.e. $q < 0$, ϵ_{xx} and ϵ_{yy} are approximately a linear function of q . At $q = -0.1$ e/atom, the strains of the 1H and 1T MoS₂ are up

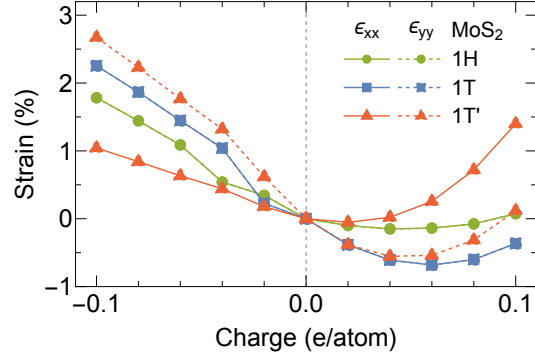


Figure 4. Strain as function of charge doping per atom of monolayer MoS₂.

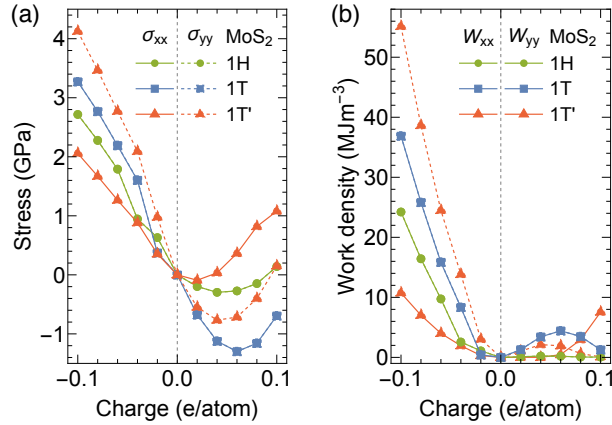


Figure 5. (a) Work density and (b) stress generated by monolayer MoS₂ plotted as function of charge (electron and hole) doping per atom.

to 1.78% and 2.25%, respectively. We can also say that 1H and 1T MoS₂ monolayers will expand isotropically ($\epsilon_{xx} = \epsilon_{yy}$). On the other hand, the 1T' MoS₂ shows an anisotropic expansion with $\epsilon_{xx} = 1.04\%$ and $\epsilon_{yy} = 2.67\%$. For the hole doping, i.e. $q > 0$, ϵ_{xx} and ϵ_{yy} are a non-linear function of q . The 1H and 1T MoS₂ monolayers show an isotropic compression with the maximum strains of about -0.15% and -0.68% at $q = 0.04 e/\text{atom}$ and $0.06 e/\text{atom}$, respectively, as shown in Fig. 4. On the contrary, the 1T' MoS₂ shows an anisotropic behaviour with the expansion strain ($\epsilon_{xx} = 1.40\%$ at $q = 0.1 e/\text{atom}$) and the compression strain ($\epsilon_{yy} = -0.55\%$ at $q = 0.04 e/\text{atom}$) along x and y directions, respectively. In this present study, the strain magnitude of 0.68% of the 1T MoS₂ by the hole doping is in a good agreement with the experimental data of about 0.6 – 0.8% [10] that making them suitable for applications in electromechanical actuators.

3.3. Actuator performance

The power of electromechanical actuators is characterized by the stress generated, which is determined by the product of the elastic modulus and the strain: $\sigma = Y\epsilon$. In Fig. 5b, we show the stress generated in monolayer MoS₂ as a function of charge doping. In the neutral case, we obtain $\sigma_{xx} = \sigma_{yy} = 0$ because $\epsilon_{xx} = \epsilon_{yy} = 0$. For the electron doping at $q = -0.1 e/\text{atom}$, we obtain $\sigma_{xx} = \sigma_{yy} = 2.72$ GPa and 3.27 GPa for the 1H and 1T structures, respectively, while $\sigma_{xx} = 2.06$ GPa and $\sigma_{yy} = 4.13$ GPa for the 1T' structure. For the hole doping, the maximum stress ($\sigma_{xx} = \sigma_{yy} = -1.30$ GPa) is found in the 1T structure at $q = 0.06 e/\text{atom}$. Our calculated σ ranging from -1.30 to 3.27 GPa for the 1T MoS₂ monolayer is higher than the experimental value for the 1T MoS₂ nanosheet (0.017 GPa) [10] due to its high Young's modulus (see Fig. 3b) and it is comparable to the carbon nanotube actuators (~ 3 GPa) [3, 37]. Our results suggest that the electron doping should be good for the actuator application of MoS₂ monolayers.

The performance of electromechanical actuators is characterized by the work density per cycle that is defined Eq. 7 as $W = Y\epsilon^2/2$. In Fig. 5a, we calculate W of the monolayer MoS₂ as a function of charge doping. For the 1T MoS₂, W is up to 36.9 MJ/m³ at $q = -0.1 e/\text{atom}$ and 4.4 MJ/m³ at $q = 0.06 e/\text{atom}$ for the electron and hole dopings, respectively, which is more than 100-1000 times that of skeleton muscle (~ 0.04 MJ/m³) [1]. These results are much higher than the experimental values for the 1T MoS₂ nanosheet (0.081 MJ/m³) [10] since Y (145 – 193 GPa) of the monolayer MoS₂ is larger than that of the MoS₂ nanosheet ($Y = 2.5 \pm 0.1$ GPa) [10]. For the 1H and 1T' structures, W at the electron doping case is higher than that of the hole doping case, which suggest that the electron doping should be good to achieve high-performance electromechanical actuators.

3.4. Electronic properties

To understand the variation of the electronic properties of the monolayer MoS₂ under charge doping, finally, we can examine the energy band structures of the monolayer MoS₂ within the range of charge doping considered in the present work. In Figs. 6a-c, we show, respectively, the calculated electronic structures of the 1H, 1T and 1T' MoS₂ along the high-symmetry points of their corresponding Brillouin zone for neutral and charge doping states. From Fig. 6a, we can see that in the neutral case, the 1H MoS₂ monolayer is an indirect-gap semiconductor (the top of valence band is at the Γ point while the bottom of conduction band is at the K point) with the band gap of about 1.59 eV. The electron (hole) doping does (does not) transform the 1H MoS₂ monolayer to be a direct-gap semiconductor. The direct (indirect) band-gap of 1H MoS₂ monolayer in the case of electron (hole) doping is about 1.25 (1.35) eV. On the other hand, from Figs. 6b and c, we find that basically in both cases of charge doping and neutral condition, the 1T MoS₂ is a metal, while the 1T' MoS₂ is a semimetal, with an exception that the 1T' MoS₂ transforms to a metal by heavy electron doping. A common interesting feature we can see in Figs. 6a-c is that the electron doping “pull down” many interlayer bands of the

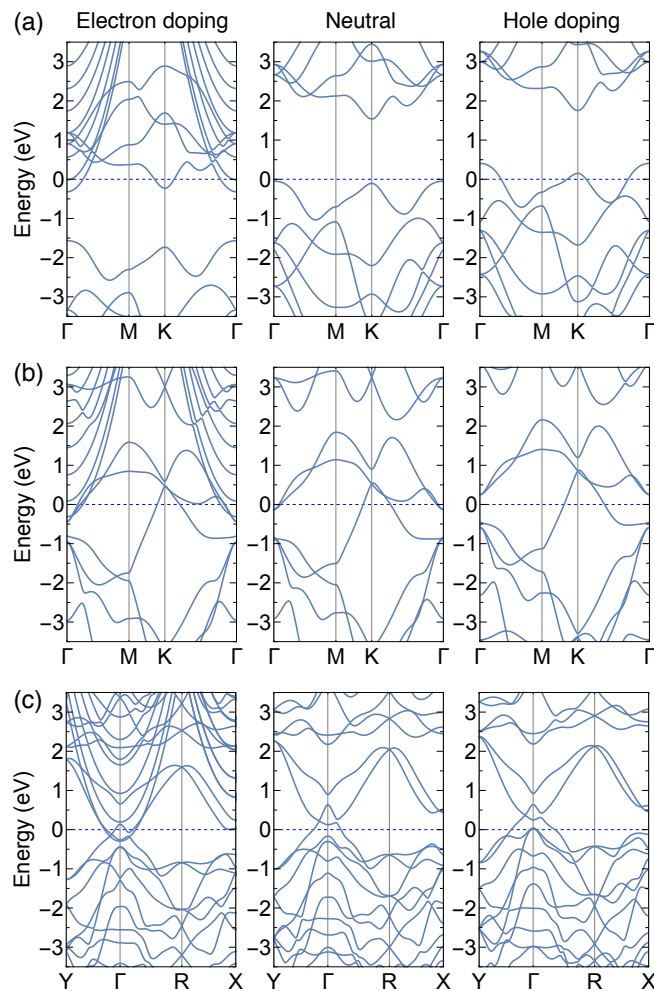


Figure 6. Energy band structures of (a) 1H, (b) 1T, and (c) 1T' MoS₂ monolayers with different electron doping ($q = -0.1 e/\text{atom}$) and hole doping ($q = +0.1 e/\text{atom}$) including those in the neutral condition ($q = 0 e/\text{atom}$). The Fermi energy (dashed line) is set to zero for all plots.

1H, 1T and 1T' MoS₂, while hole doping do not. Such a phenomenon might contribute to the higher performance of MoS₂ electromechanical actuators by the electron doping rather than the hole doping, as shown previously in Figs. 5a and b.

4. Conclusions

We have performed a first principles theoretical study on the actuator performance and on the electronic structure as a function of charge doping for the 1H, 1T and 1T' MoS₂ monolayers. We find that the work density per cycle and stress generated in 1T and 1T' MoS₂ monolayers are relatively larger than those in 1H MoS₂ monolayer. This excellent electromechanical performance originate from the electrical conductivity of the metallic 1T and semimetallic 1T' structures high Young's modulus of about 150–200 GPa under charge doping. The results obtained also reveal that the 1H and 1T MoS₂ show the

actuator isotropy, while 1T' MoS₂ shows the actuator anisotropy, which implies that researchers can have more freedom to choose the best MoS₂ structures depending on the isotropic or anisotropic electromechanical applications.

5. Acknowledgements

N.T.H. and A.R.T.N acknowledge the Interdepartmental Doctoral Degree Program for Multidimensional Materials Science Leaders under the Leading Graduate School Program in Tohoku University. R.S. acknowledges JSPS KAKENHI Grant Numbers JP25107005 and JP25286005.

- [1] Madden J D W, Vandesteeg N A, Anquetil P A, Madden P G A, Takshi A, Pytel R Z, Lafontaine S R, Wieringa P A and Hunter I W 2004 *IEEE J. Oceanic Eng.* **29** 706–728
- [2] Baughman R H, Cui C, Zakhidov A A, Iqbal Z, Barisci J N, Spinks G M, Wallace G G, Mazzoldi A, De Rossi D, Rinzler A G, Jaschinski O, Roth S and Kertesz M 1999 *Science* **284** 1340–1344
- [3] Hung N T, Nugraha A R T and Saito R 2017 *Carbon* **118** 278–284
- [4] Rogers G W and Liu J Z 2011 *J. Am. Chem. Soc.* **133** 10858–10863
- [5] Xie X, Bai H, Shi G and Qu L 2011 *J. Mat. Chem.* **21** 2057–2059
- [6] Yu M F, Files B S, Arepalli S and Ruoff R S 2000 *Phys. Rev. Lett.* **84** 5552
- [7] Hung N T, Truong D V, Thanh V V and Saito R 2016 *Comput. Mater. Sci.* **114** 167–171
- [8] Weissmüller J, Viswanath R N, Kramer D, Zimmer P, Würschum R and Gleiter H 2003 *Science* **300** 312–315
- [9] Jin H J, Wang X L, Parida S, Wang K, Seo M and Weissmüller J 2009 *Nano Lett.* **10** 187–194
- [10] Acerce M, Akdoğan E K and Chhowalla M 2017 *Nature* **549** 370–373
- [11] Lin Y C, Dumcenco D O, Huang Y S and Suenaga K 2014 *Nat. Nanotech.* **9** 391–396
- [12] Naylor C H, Parkin W M, Ping J, Gao Z, Zhou Y R, Kim Y, Streller F, Carpick R W, Rappe A M, Drndic M, Kikkawa J M and Johnson A T C 2016 *Nano Lett.* **16** 4297–4304
- [13] Li T 2012 *Phys. Rev. B* **85** 235407
- [14] Bertolazzi S, Brivio J and Kis A 2011 *ACS Nano* **5** 9703–9709
- [15] Castellanos-Gomez A, Poot M, Steele G A, van der Zant H S J, Agraït N and Rubio-Bollinger G 2012 *Adv. Mater.* **24** 772–775
- [16] Sun X, Wang Z, Li Z and Fu Y Q 2016 *Sci. Repor.* **6** 26666
- [17] Fan X L, Yang Y, Xiao P and Lau W M 2014 *J. Mater. Chem. A* **2** 20545–20551
- [18] Giannozzi P *et al.* 2009 *J. Phys. Condens. Matter* **21** 395502
- [19] Lejaeghere K *et al.* 2016 *Science* **351** aad3000
- [20] Perdew J P, Burke K and Ernzerhof M 1996 *Phys. Rev. Lett.* **77** 3865
- [21] Monkhorst H J and Pack J D 1976 *Phys. Rev. B* **13** 5188
- [22] Broyden C G 1970 *IMA J. Appl. Math.* **6** 76–90
- [23] Fletcher R 1970 *Comput. J.* **13** 317–322
- [24] Goldfarb D 1970 *Math. Comput.* **24** 23–26
- [25] Shanno D F 1970 *Math. Comput.* **24** 647–656
- [26] Dal Corso A 2016 *J. Phys. Condens. Matter* **28** 075401
- [27] Young P A 1968 *J. Phys. D: Appl. Phys.* **1** 936
- [28] Wang L, Kutana A, Zou X and Yakobson B I 2015 *Nanoscale* **7** 9746–9751
- [29] Spinks G M and Truong V T 2005 *Sens. Actuators A: Phys.* **119** 455–461
- [30] Du Y, Maassen J, Wu W, Luo Z, Xu X and Peide D Y 2016 *Nano Lett.* **16** 6701–6708
- [31] Jiang J W and Park H S 2016 *Nano Lett.* **16** 2657–2662
- [32] Wang H, Li X, Li P and Yang J 2017 *Nanoscale* **9** 850–855
- [33] Baughman R H, Shacklette J M, Zakhidov A A and Stafstrom S 1998 *Nature* **392** 362
- [34] Hung N T, Nugraha A R T and Saito R 2017 *Carbon* **125** 472–479

- [35] Rho J Y, Ashman R B and Turner C H 1993 *J. Biomechanics* **26** 111–119
- [36] Sun G, Kürti J, Kertesz M and Baughman R H 2002 *J. Am. Chem. Soc.* **124** 15076–15080
- [37] Qu L, Peng Q, Dai L, Spinks G M, Wallace G G and Baughman R H 2008 *MRS Bull.* **33** 215–224